Turbulence in a Localized Puff in a Pipe

Alexander Yakhot, Yuri Feldman, David
Moxey, Spencer Sherwin and George Em
Karniadakis

Abstract We have performed direct numerical simulations of a spatio-temporally intermittent flow in a pipe for $Re_m = 2250$. From previous experiments and simulations of pipe flow, this value has been estimated as a threshold when the average speeds of upstream and downstream fronts of a puff are identical [1], [2]. We investigated the structure of an individual puff by considering three-dimensional snapshots over a long time period. To assimilate the velocity data, we applied a conditional sampling based on the location of the maximum energy of the transverse (turbulent) motion. Specifically, at each time instance, we followed a turbulent puff by a three-dimensional moving window centered at that location. We collected a snapshot-ensemble (10000 time instances, snapshots) of the velocity fields acquired over $T = 2000D/U$ time interval inside the moving window. The cross-plane velocity field inside the puff showed the dynamics of a developing turbulence. In particular, the analysis of the cross-plane radial motion yielded the illustration of the production of turbulent kinetic energy directly from the mean flow. A snapshot-ensemble averaging over 10000 snapshots revealed azimuthally arranged large-scale (coherent) structures indicating near-wall sweep and ejection activity. The localized puff is about 15-17 pipe diameters long and the flow regime upstream of its upstream edge and downstream of its leading edge is almost laminar. In the near-wall

A. Yakhot
Department of Mechanical Engineering, Ben-Gurion University, Beersheva 84105, Israel, E-mail: yakhot@bgu.ac.il
Y. Feldman
Department of Mechanical Engineering, Ben-Gurion University, Beersheva 84105, Israel
D. Moxey
College of Engineering Mathematics and Physical Sciences, University of Exeter, N Park Rd, Exeter EX4 4QF, UK
S. Sherwin
Department of Aeronautics, Imperial College London, South Kensington Campus, London SW7 2AZ, UK
G. E. Karniadakis
Division of Applied Mathematics, Brown University, Providence, RI 02912, USA

region, despite the low Reynolds number, the turbulence statistics, in particular, the distribution of turbulence intensities, Reynolds shear stress, skewness and flatness factors, become similar to a fully-developed turbulent pipe flow in the vicinity of the puff upstream edge. In the puff core, the velocity profile becomes flat and logarithmic. It is shown that this "fully-developed turbulent flash" is very narrow being about two pipe diameters long.

1 Introduction

More than forty years ago, experiments conducted in a pipe for mixed laminar-turbulent flows at the range of Reynolds numbers of $2000 < Re_m < 2700$ revealed turbulent self-sustained confined regions, surrounded by a laminar flow and convected downstream [3] and [4]. The authors referred to these regions as puffs and slugs. It was found that with an increase in the Reynolds number, puffs increase in size, turn into slugs, split and even recombine. For reviews on the transition to turbulence in a pipe, together with a thorough analysis of the flow structure and dynamics of a puff, see [1], [2] and [5]. In [6], it was shown that at the upstream edge of the puff, where the laminar flow undergoes transition to turbulence, pairs of counter rotating streamwise vortices are observed which were referred to as the legs of large hairpin vortices. In [7], a control mechanism was developed to eliminate turbulence in laminar-turbulent intermittent flows by attenuating the mean shear and, thus, preventing the energy transfer from the mean flow into turbulent eddies.

Pioneering research on the puff concluded that it "*maintains itself indefinitely at around $Re_m = 2200$*" and called such turbulent patches *equilibrium*, meaning that they are self-sustaining substances of constant size. Nevertheless, the very existence of so-called equilibrium puffs was not an obvious fact until recent experimental and numerical studies on the lifetime of turbulent puffs have emerged in the last decades [8], [9]. In these studies, the lifetime is estimated in terms of probability of finding a turbulent flow state at a time t as a function of the Reynolds number. In [8] and [9], puffs and, in particular, splitting events, have been studied on the basis of both numerical and experimental results.

Direct numerical simulations (DNS) of turbulent-laminar states in pipe flows at transitional Reynolds numbers have been carried out for axially periodic pipes of length L and diameter D [8], [9], [10], [11], [12] and [13]. Extensive DNS in pipes of different lengths up to 125 diameters have shown that below $Re \simeq 2300$, turbulence is observed in the form of longtime localized puffs and their size is independent of pipe length [9]. In [10], DNS of a puff has been carried out at a Reynolds number of $Re_m = 2200$ in a pipe of $L = 16\pi D$. The results show that the flow is completely laminar outside the puff, while the leading and upstream edges of a puff travel with a constant velocity. The conclusions derived from DNS results in [11] are that localized puffs indeed exist in long pipes at $Re_m = 2200, \; 2350$. In [11], for $Re_m = 2200$, the authors

confirmed that a streamwise period of $L = 8\pi D$ is close to the minimal admissible pipe length to predict typical puff-like structures, as they previously established in [12]. The simulations in [11] have been carried out for a very longtime interval of about $T = 2000D/U_m$. The fluid dynamics of a localized puff, observed in an axially periodic pipe ($L = 8\pi D$) at $Re_m = 2226$, was discussed in [13]. These authors reported the results collected over not a long-time interval of $T = 560D/U_m$, and questioned the puff's endless existence. Indeed, one of the conclusions of [9] is that an "equilibrium" (or isolated) puff, as was seen by [4] and aftermath referred to in many DNS studies, does not exist forever. In [9], the authors have shown that after some finite (but very large) lifetime, a given puff will either decay or split. Recently, a summary of extensive experimental and numerical studies led to the conclusion that for Reynolds numbers $Re_m \simeq 2250$, turbulent puffs are localized, in the sense that their upstream and downstream front speeds are identical, and, therefore, their size does not change for reasonably long but finite times [14].

The objective of this work is to obtain long-time statistical and average properties of the velocity field inside a localized turbulent puff travelling through a pipe. To this end, we collected a velocity database over the time interval of $T = 2000D/U_m$ in a moving window (co-moving reference frame) linked with a puff.

2 Computational setup

In this article we report results from a DNS of a turbulent puff in pipe flow for $Re_m = 2250$, where the Reynolds number is defined as $Re_m = U_m D/\nu$, with $U_m = 1$ the bulk velocity, $D = 1$ the pipe diameter and a pipe length of $L = 8\pi D$ (hereafter referred as $L = 25D$). The numerical simulation follows the approach described and validated in [8], using the hybrid spectral-element–Fourier pseudospectral code *Semtex* [15], which evolves the incompressible Navier-Stokes equations using a second-order splitting timestepping scheme proposed in [16] with a timestep size of $\Delta t = 2 \times 10^{-3}$; the data was collected every 100 time steps. Periodic boundary conditions are applied in the streamwise direction and no-slip conditions are imposed at the pipe wall. We use a spectral element mesh comprising 78 elements at a high polynomial order of $P = 12$ in circular cross-sections of the domain, with appropriate boundary layer resolution near the pipe wall. In the streamwise direction, we use 512 Fourier collocation points (256 Fourier modes), giving a total resolution of around 6.7 million degrees of freedom for the simulation per field variable. The flow is driven through the use of a constant mass-flow imposing a bulk velocity $U_m = 1$ described in [17], [18] and therefore enforcing a prescribed value of Re. The initial puff configuration arises from the $L = 25D$ reverse transition studies described in [8], where the simulation was initially evolved for 200 non-dimensional time units before collection of statistics, to

Fig. 1 DNS of a turbulent puff in pipe flow at $Re_m = 2250$. Iso-surfaces of the total kinetic turbulent energy $e_{tot} = e_\perp + e_z$ plotted in a 4D-length window, centered around the cross-section S32 with $e_\perp^{(max)}$.

allow any transient effects to diminish due to the slightly higher resolution of these simulations.

In this paper, the results are presented using cylindrical coordinates $\mathbf{x} = (r, \theta, z)$ and the corresponding velocities are denoted by $\mathbf{u} = [u_r(\mathbf{x}, t), u_\theta(\mathbf{x}, t), u_z(\mathbf{x}, t)]$. We collected a *snapshot-ensemble* of 10,000 snapshots of the flow field inside a moving window shown in Figure 1, that is, over the time interval $T = 2000D/U_m$. The moving window consists of 63 cross-sectional slices, denoted as S1, S2,..., S63, corresponding to the grid points in the axial direction with $\Delta z = 25D/512$. In wall units, this means $\Delta z^+ \approx 7.8$. This is a quite high resolution (compared to $\Delta z^+ \approx 24$ in [11]) and no abrupt unphysical changes were detected. A 4D-width moving window is centered around the location where the kinetic energy of the instantaneous transverse motion $e_\perp = \sum_{CS} (u_r{}^2 + u_\theta{}^2)$ is maximal; $\sum_{CS}$ denotes the summation over all cross-sectional points. Since the transverse motion is possible only for turbulent flows, the location with $e_\perp^{(max)}$ is the best indication of the locally turbulent regime. The streamwise fluctuating velocity component is defined as $w = u_z - \overline{u}_z$, where (and hereafter) a bar-sign denotes the snapshot-ensemble averaging. Consequently, $e_z = \sum_{CS} w^2$ and $\overline{e}_z$ are the kinetic energy of the streamwise velocity fluctuations and its snapshot-ensemble average.

Figure 2 shows three-dimensional iso-surfaces obtained by the snapshot-ensemble averaging of the radial u_r-velocity component inside the puff. We focus on the developing transverse (cross-plane) motion inside the puff which plays a special role in the onset of turbulence.

Figure 3 shows the time trace of the centerline velocity measured at a fixed point in the laboratory reference frame in which the pipe is stationary. The laminar (Poiseuille) centerline velocity normalized by U_m is 2. The deficit in the streamwise velocity is visible, that is, the flow behind the puff is not completely relaminarized. This results from the fact that the periodic computational domain is of insufficient length. Its possible influence on our findings will be discussed below. A steep pattern of the time-trace indicates a sharp interface between the laminar and turbulent regions at the puff upstream edge vicinity. For the observer moving with the puff, the high speed laminar fluid enters the puff entraining the slow near-wall fluid.
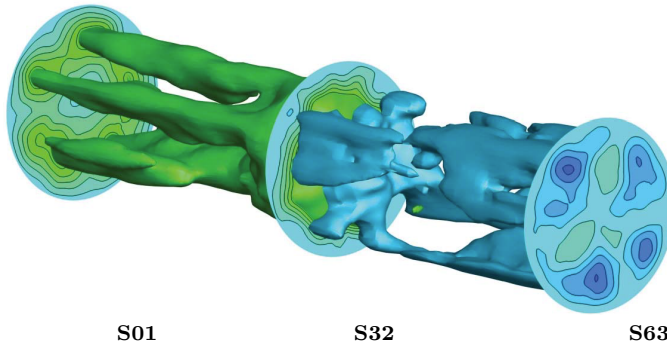
Fig. 2 Three-dimensional iso-surfaces of the averaged u_r-velocity in a moving window of the width $\pm 2D$; at each time instance, t, the window is centered around the cross-section S32 with $e_\perp^{(max)}$.
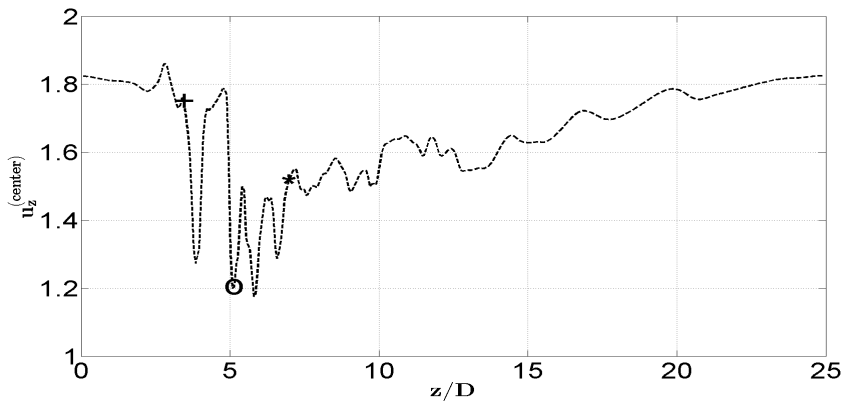
Fig. 3 Typical time trace of the centerline velocity. The symbols are an example of a single snapshot in a moving window reference frame: an asterisk (*) for the leading edge (S63), an open circle (o) for the middle section (S32) and a plus sign (+) for the trailing edge (S01) of the moving window; here, $z/D = 5$ in a laboratory frame of reference corresponds to $z/D = 0$ in the moving reference frame linked with a puff.

3 Results

The results presented here refer to different cross-sections of the moving window, in the center of which (S32, marked by a circle in figure 3) the energy of the transverse (turbulent) motion is maximum. Note that with respect to the moving window, the upstream edge of the puff is slightly upstream. In other words, in section S01 (the trailing edge of the moving window, marked by a plus sign in figure 3), the flow regime is in the onset of turbulence[1]. In the moving window reference frame, $z = 0$ denotes the S32 cross-section where

---

[1] Thus, when we say *"at the moving window trailing edge S01,"* it also implies *"slightly downstream of the upstream edge of the puff."*

the in-plane kinetic energy $e_\perp$ is maximum and $z = -2D$ denotes the moving window trailing edge S01.

We present the snapshot-ensemble averaged results collected over $2000D/U_m$ time units. It is plausible that the extremely long-time averaging should produce azimuthally symmetric properties. Indeed, the azimuthally asymmetric structures discussed below point to an insufficient averaging interval. On the other hand, it indicates structures' robustness.

3.1 Cross-plane flow structures

The cross-plane motions play an important role in turbulence production. In the framework of the Reynolds decomposition approach, for the considered flow, the leading terms of the Reynolds-stress budget equations are [19]:

$$P_{r,z} \simeq -\overline{u_r^2}\frac{\partial \overline{u_z}}{\partial r}, \quad P_{z,z} \simeq -2\overline{wu_r}\frac{\partial \overline{u_z}}{\partial r}, \tag{1}$$

where $P_{r,z}$ and $P_{z,z}$ denote the production of the Reynolds stress $\overline{wu_r}$ and the kinetic energy of the streamwise fluctuations $\overline{w^2}$, respectively. The important consequence of the Reynolds stresses budget equations is that the production of turbulent kinetic energy directly from the mean flow occurs in the equation for $\overline{w^2}$, while $\overline{u_r^2}$ and $\overline{u_\theta^2}$ receive their energy from the pressure-strain interaction terms. For shear flows, the w component has more energy, while the non-linear pressure-strain interaction provides a redistribution of the energy between three directions. In order to start this process, the radial component u_r must be generated. Indeed, from (1), u_r is needed to generate the Reynolds shear stress $\overline{wu_r}$, which, in turn, generates the kinetic energy of the streamwise w component. Thus, from the point of view of sustaining the turbulence, the cross-plane radial motion indicates the onset of turbulence energy production.

Figure 4 shows typical contours of the instantaneous streamwise (u_z, a), fluctuating streamwise (w, b) and radial (u_r, c) velocity components at the moving window trailing edge S01. Figure 4a shows the contours of the streamwise velocity u_z. The wavy form near the wall indicates the entrainment of a low-speed fluid toward the center. Note that at the moving window trailing edge (S01), the radial movement is restricted mostly to the wall region, while at the pipe center the flow remains almost undisturbed.

In figure 4b (the moving window trailing edge), there are clearly visible three footprints at locations marked by 1, 2 and 3. We note radial motion of low-speed fluid from the wall at these locations (figure 4c). As will be shown in the Discussion section, its origin is explained by the formation of axial vorticity ω_z. From figure 4b, strong negative fluctuations of the streamwise velocity led to a significant momentum deficit, and high speed fluid swept toward the wall to compensate this deficit ($r = 0.15$, $\theta = 180°$). As a result, near the wall,

alternating regions of high- and low-speed streaks[2] have appeared (figure 4b , $90° < \theta < 225°$).

From figure 5b, two diameters downstream, the two footprints have been almost destroyed and 5-6 low-speed streaks ($w < 0$) are clearly seen near the wall. Two diameters downstream, in figure 5e, this is even more pronounced.

Figure 4c shows two counter-rotating streamwise vortices. Two diameters downstream, in figure 5c, the intensive turbulent motion in the core is associated with penetration of the fluid lifted-up from the wall and was entrained by a high-speed flow. Consequently, the scale bar in figure 5c shows an increase in the radial motion intensity by a factor of five.

The development of flow structures inside a puff shown in figures 4 and 5 agrees with that presented in [6] in terms of the axial vorticity, total axial velocity, and cross-plane vorticity.

Figure 6a shows the ensemble-averaged radial velocity component, $\overline{u}_r$. Here, the entrainment of low-speed fluid lifted-up from the wall is manifested by five clear local $\overline{u_r}-$maxima. The azimuthal quasi-periodicity of $\overline{u_r}$ in figure 6a can mean the existence of the travelling waves which were observed experimentally and numerically in studies on laminar-turbulent transition of pipe flows [20]. In [20], a velocity field measured in a cross-sectional plane close to the upstream edge of a puff is shown in figure 2A. This location is close to the cross-section S01 in our study. The pattern in figure 6a is remarkably similar to that presented in [20], where turbulent structures were revealed by recording the velocity field in a series of 1000 contiguous measurements. The fact that the structures in figure 6a "survived" the snapshot-ensemble averaging is in line with the finding that spatial features of these wave states persist over large time intervals [20].

The snapshot-ensemble averaging clearly indicated the azimuthally arranged structures, but this does not explain how these structures correlate, if at all, in time. Figure 6 shows a two-point azimuthal correlation coefficient of the radial velocity component, $R_{u_r,u_r}(\theta, \theta_0)$ obtained from 10000 snapshots for a given radius. Azimuthal correlations for $r = 0.33$ and $\theta_0 = 48°$, $120°$ and $278°$, corresponding to three locations with maximum $\overline{u_r}$ (figure 6a), are shown in figures 6b-d. Here, two negative minima surrounding the positive maximum of R_{u_r,u_r} indicate the locations of the corresponding outward ejection of low-speed fluid, which manifests itself in the form of a wave in figure 6a. Thus, we *ad hoc* assume that the limits $|R_{u_r,u_r}| > 0.2$ indicate well correlated data[3]. For a puff, a correlation coefficient larger than 0.1 was considered as a "good" correlation in [21]. As for the range $0.1 < |R_{u_r,u_r}| < 0.2$, we consider these data as correlated. From figure 6b, $R_{u_r,u_r}(330°, 48°) = 0.1$ at $r = 0.33$, which means that these two sweeping events (figure 6a) correlate. There is no correlation between other sweeping events shown in figure 6a.

---

[2] "Low-speed" ($w < 0$) and "high-speed" ($w > 0$) are usually used as relative terms, and refer to deviations from the mean streamwise velocity value at that location.

[3] In this study, we take into account that the near-wall ejection and sweeping correlate and are spatially close. Therefore, the computed range of $|R_{u_r,u_r}| > 0.2$ leads us to consider these data as well correlated.
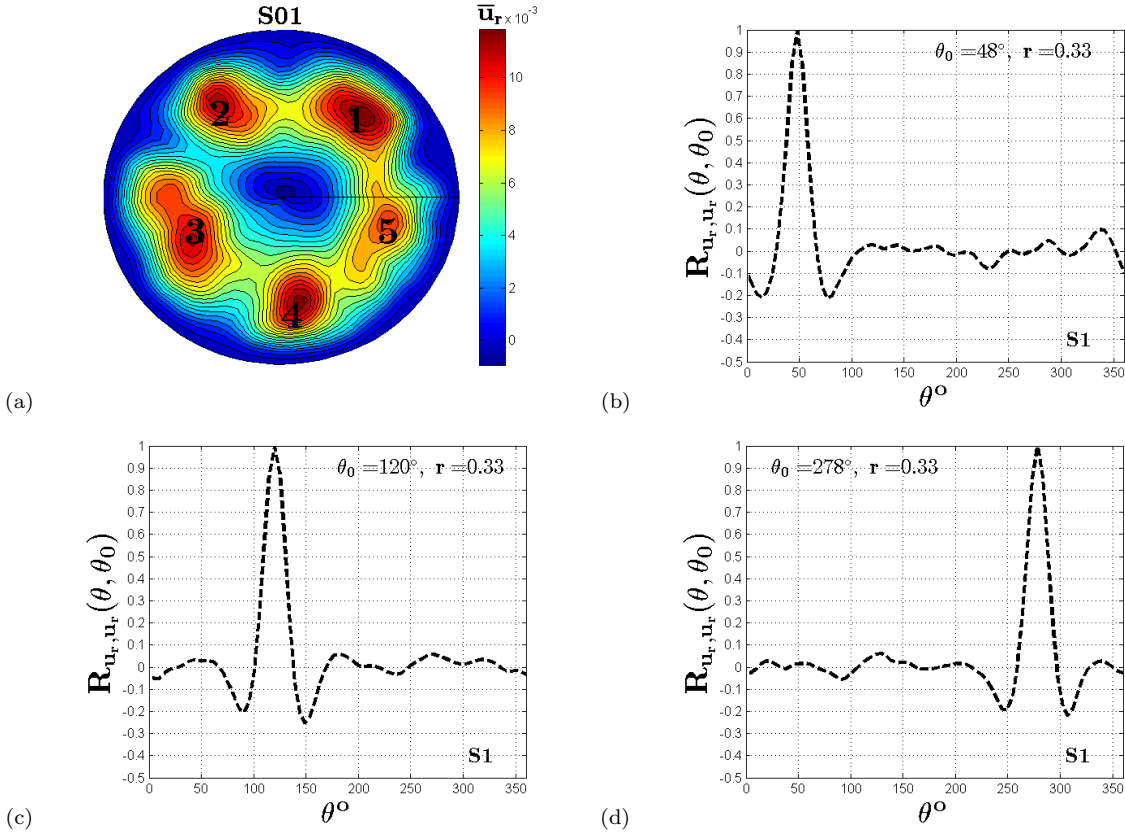
(a)

(b)

(c)
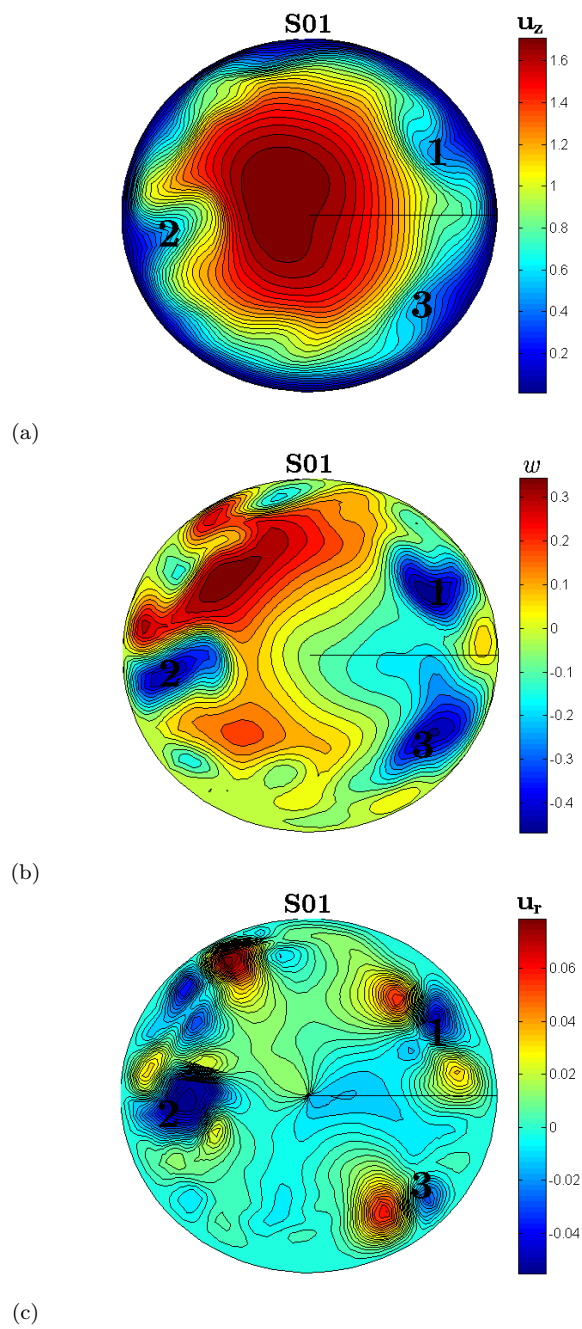
Fig. 4 Typical contours of the instantaneous streamwise (u_z, a), fluctuating streamwise (w, b), and radial (u_r, c) velocity components at the moving window trailing edge S01.
.
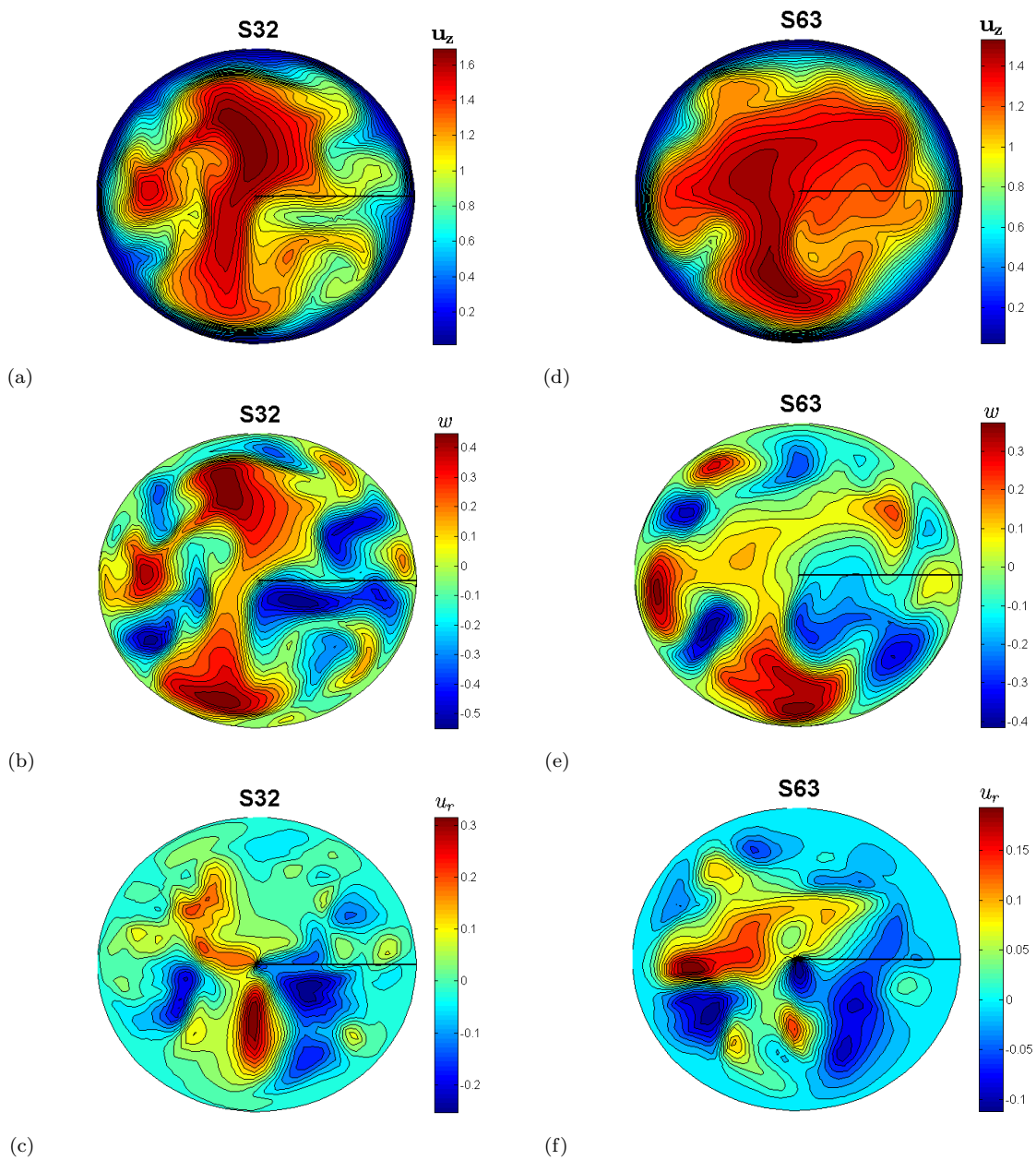
Fig. 5 Typical contours of the instantaneous streamwise (u_z), fluctuating streamwise (w), and radial (u_r) velocity components at S32 (a-c) and S63 (d-f) cross-sections along the moving window.
.

(a)

(b)

(c)

(d)

Fig. 6 Trailing edge of the moving window (S1). Contours of the snapshot-ensemble averaged radial velocity ($\overline{u}_r$) and the two-point correlation coefficient R_{u_r,u_r} (b-c) calculated in the azimuthal direction for specified radius r; three θ_0 locations correspond to maximum values of $\overline{u_r}$.
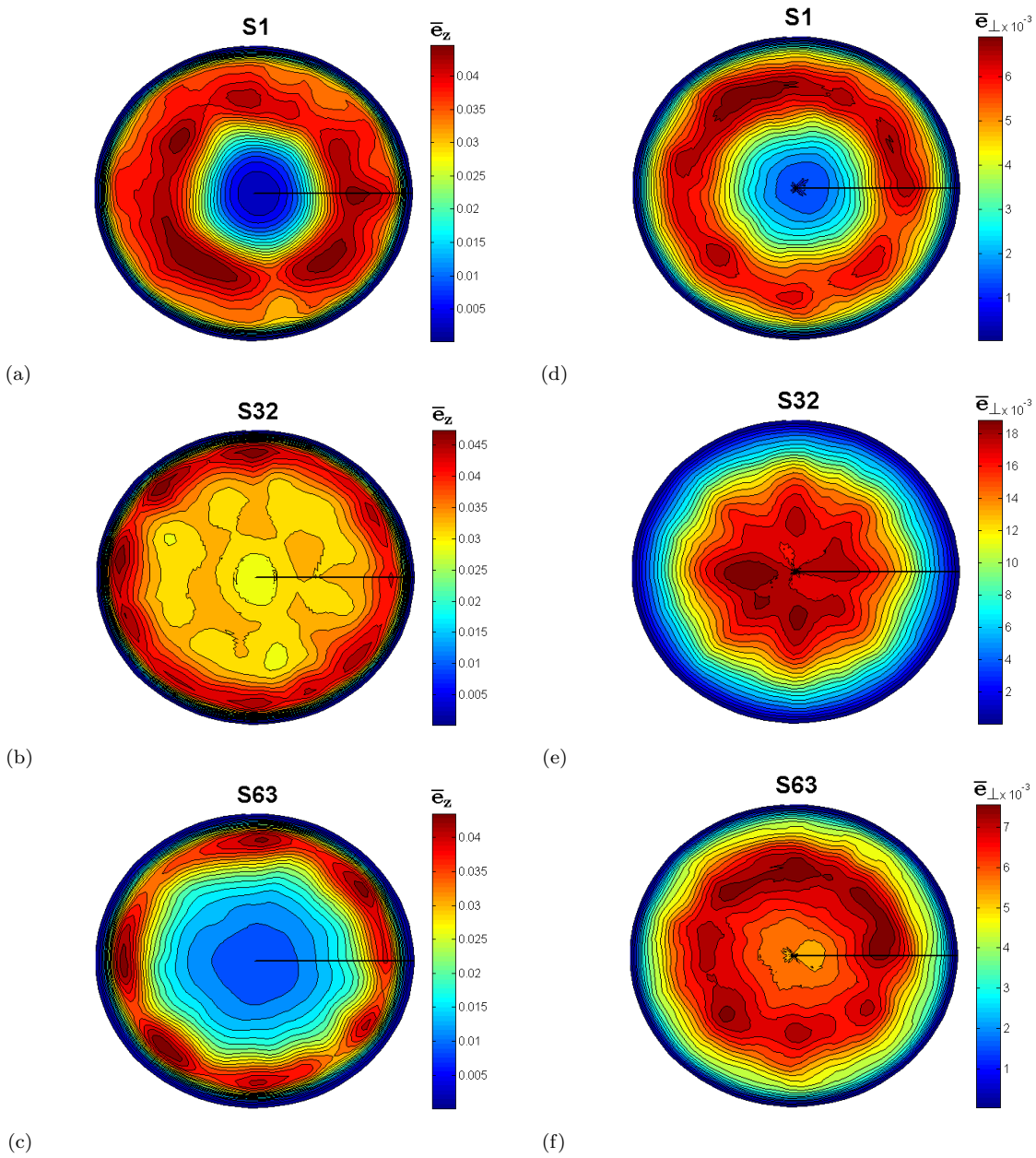
.

Figure 7 shows contours of the snapshot-ensemble averaged kinetic energy of streamwise ($\overline{e}_z$, a-c) and transverse ($\overline{e}_\perp$, d-f) fluctuations at different cross-sections along the moving window. Surprisingly, near the wall, $0.4 < r/D < 0.5$, the magnitude of the streamwise kinetic energy, $\overline{e}_z$, is practically the same at all three cross-sections (figure 7a-c) along the puff. This observation implies that the near-wall streaks are very persistent. In the pipe core, $0 < r/D < 0.3$, the picture is completely different. From figure 4c, at the moving window trailing edge (S01), in the pipe core there is still no strong movement in the radial direction to generate turbulent kinetic energy (Eq. 1). This is because the low-speed fluid lifted up from the near-wall region did not reach the center. Therefore, the $\overline{e}_z$-energy in the pipe core there is insignificant (figure 7a). Two diameters downstream between the cross-sections S01 and S32 strong radial motion (figure 5c) and, apparently, high mean shear, led to a significant increase of the streamwise turbulent energy, $\overline{e}_z$, in the pipe core (figure 7b). This

is in full agreement with the fact that in this region the cross-sectionally integrated turbulence production exceeds the integrated dissipation [3] and [14]. Further downstream, between the S32 and S63 cross-sections, the streamwise kinetic energy decreases considerably for two reasons. Firstly, in accordance with the kinetic energy balance, the pressure-strain term takes energy away from the streamwise component to redistribute it into the cross-plane energy, $\overline{e_\perp}$, as demonstrated in figures 7e and 7f. Secondly, as will be shown, the mean velocity profile becomes more flat and, consequently, the $\overline{e_z}$-energy production by mean shear decreased (Eq. 1).
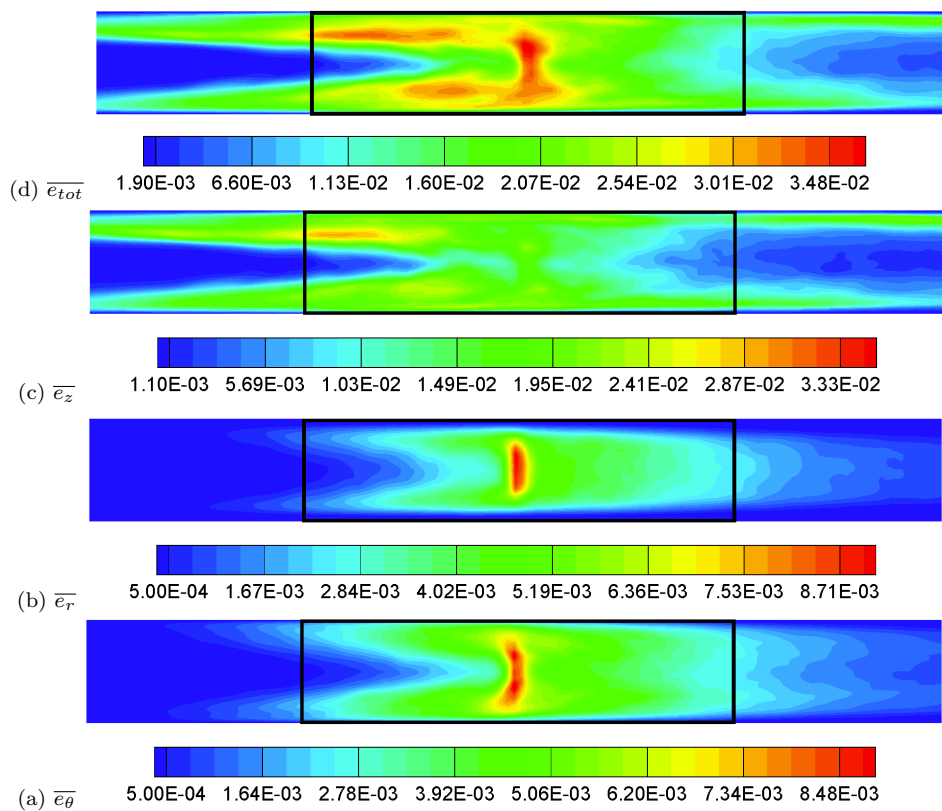
Figures 7a-c show a wavy pattern in $\overline{e}_z$-energy distribution with local maxima in the azimuthal direction. This pattern indicates the azimuthal quasi-periodicity, and in S32 and S63, this feature is even more pronounced (figures 7b and 7c). In the pipe core, due to the fact that the cross-plane energy $\overline{e_\perp}$ is fed by $\overline{e_z}$, the wavy patterns in figures 7e and 7c are completely correlated when the decrease of $\overline{e_z}$ in the radial direction is followed by an increase of $\overline{e_\perp}$. Note that the same pattern was observed in a puff [6] and in fully-developed turbulent pipe flow [22].

Figure 8 shows the distributions of the snapshot-ensemble averaged turbulence kinetic energy in the (r, z)-plane. Upstream of the moving window trailing edge (S01), the energy is extracted from the high-speed laminar flow by low-speed fluid ejected outward from the wall. The energy of streamwise fluctuations $\overline{e_z} = \overline{(w - \bar{w})^2}$ is also generated in the near-wall region, but the major mechanism for the sustaining puff turbulence is the upstream entering of the high-speed laminar fluid. As a result, up to the middle section, a considerable overproduction of the $\overline{e_z}$ energy is observed in $0.25 < r/D < 0.35$ (figure 8c) that is redistributed between the the cross-plane $\overline{e_r}$ and $\overline{e_\theta}$ energies up to the moving window leading edge.

To conclude the results presented in this section, the 2D-length part of the moving window between the cross sections S01 and S32 (just upstream of the puff upstream edge) is characterised by a strong turbulent energy production. Further downstream, between S32 and S63, the streamwise e_z-energy is redistributed into the cross-plane energies, e_r and e_θ.

Fig. 7 Contours of the snapshot-ensemble averaged energy of streamwise ($\overline{e}_z$, a-c) and transverse ($\overline{e}_\perp$, d-f) fluctuations at different cross-sections along the moving window.
.

(d) $\overline{e_{tot}}$ 1.90E-03 6.60E-03 1.13E-02 1.60E-02 2.07E-02 2.54E-02 3.01E-02 3.48E-02

(c) $\overline{e_z}$ 1.10E-03 5.69E-03 1.03E-02 1.49E-02 1.95E-02 2.41E-02 2.87E-02 3.33E-02

(b) $\overline{e_r}$ 5.00E-04 1.67E-03 2.84E-03 4.02E-03 5.19E-03 6.36E-03 7.53E-03 8.71E-03

(a) $\overline{e_\theta}$ 5.00E-04 1.64E-03 2.78E-03 3.92E-03 5.06E-03 6.20E-03 7.34E-03 8.48E-03

Fig. 8 Distributions of the snapshot-ensemble averaged turbulence energy in the 8D-width part of the pipe centered around the moving window: (a) the energy of transverse azimuthal fluctuations $\overline{e_\theta}$; (b) the energy of transverse radial fluctuations $\overline{e_r}$; (c) the energy of longitudinal fluctuations $\overline{e_z}$; (d) the total energy $\overline{e_{tot}} = \overline{e_z} + \overline{e_r} + \overline{e_\theta}$.

3.2 Mean flow properties

In this section, we present the long-time statistical and average properties of
the velocity field inside the moving window. Figure 9 shows the streamwise
velocity profiles averaged over 10,000 snapshots and over 78 azimuthal points
for each radius (r): $W(r)$ normalized by the mean velocity (a); $W_+(y_+)$ nor-
malized by a shear velocity, in wall units (b). A flow regime similar to the
developed turbulence, wherein the velocity profile becomes flat in the core
(figure 9a) and logarithmic (figure 9b), develops along the moving window,
which takes the downstream distance of several pipe diameters. An observer
sitting in the middle section (S32) of the moving window, will see a sharp
upstream interface between the almost laminar and turbulent states when the
velocity profile rapidly flattens (figure 9a, S01 vs. S32 curves). On the other
hand, two diameters downstream, the profile remains flat (figure 9a, S32 vs.
S63 curves). The localized puff is a confined turbulent structure with an ax-
ial size of 12÷15D. Inside the puff, the moving window presents a coherent
picture of the flow dynamics development, in accordance to which a laminar
flow undergoes transition to turbulence before relaminarising further down-
stream. The results in figure 9 show the existence of a narrow 4D-length slot,
wherein the velocity profile becomes flat in the pipe core and logarithmic. It
is noteworthy that in the middle section (S32) the log-profile is quite long,
although its slope is large, $\kappa^{-1} = 4.5$, instead of the von Karman constant
$\kappa^{-1} \simeq 2.5$. A detailed discussion of this subject is beyond the scope of this
study. Here, we speculate that the presence of the log profile is explained by
the balance between generation and dissipation of turbulent energy, while its
extend practically to the pipe center can be related to the overproduction of
energy there.

For a fully-developed turbulent flow in a pipe or channel, in order to com-
pare the validity of the universal logarithmic ($W_+ = \kappa^{-1} \ln y_+ + B$) or power-
law ($W_+ = Cy_+^\alpha$) velocity profile, it is common to calculate the indicator
functions as follows [23]:

$$\beta = y_+ \frac{dW_+}{dy_+} \quad \text{and} \quad \alpha = \frac{y_+}{W_+} \cdot \frac{dW_+}{dy_+}. \tag{2}$$

Hence, if there is a log layer or a power law layer, both indicator function
curves will have a plateau indicating the values of $\beta = \kappa^{-1}$ or α. Figure 10a
shows the distribution of α. Over the "universal" region, α very slowly linearly
increases, namely, $\alpha = 0.27 \pm 1\%$. The log-layer indicator β varies also linearly,
but over a wider range, $\beta = 4.5 \pm 0.4$ (figure 10b). For comparison, the DNS
results of a turbulent channel flow (N. Nikitin, private communication) are
also shown in figure 10.

(a)

(b)
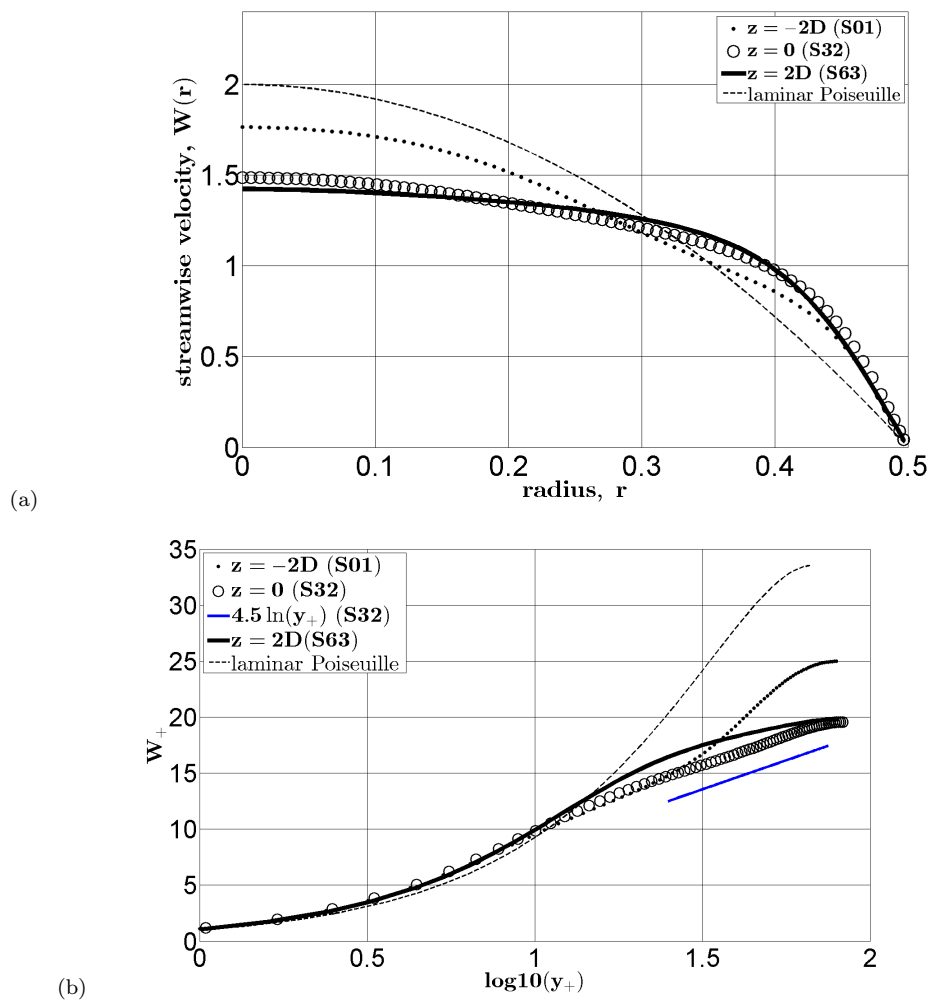
Fig. 9 The streamwise velocity profiles: (a) $W(r)$ normalized by the mean velocity; (b) $W_+(y_+)$ normalized by a shear velocity, in wall units. $W_{+,lam}^{(center)} = (Re_m/2)^{1/2} = 33.5$
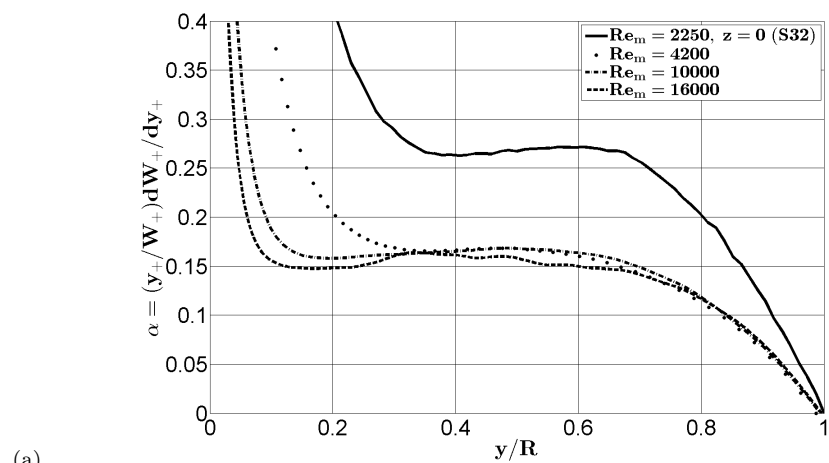
(a)
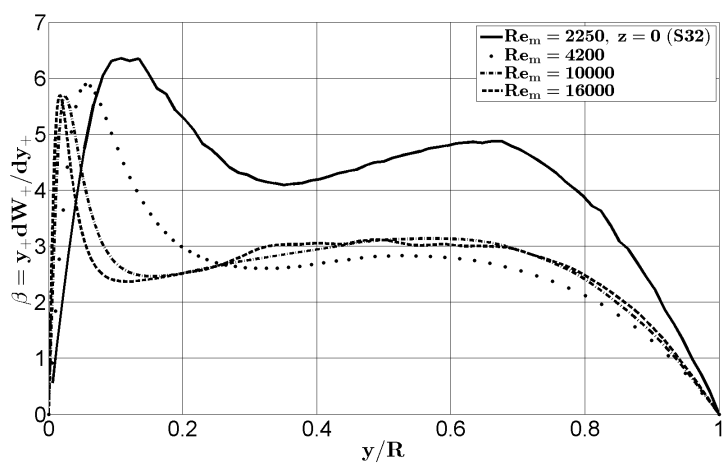
(b)

Fig. 10 $\alpha = \frac{y_+}{W_+} \cdot \frac{dW_+}{dy_+}$ a power law indicator (a); $\beta = y_+ \frac{dW_+}{dy_+}$ a log-profile indicator; y - distance to the wall; $Re_m = 4200, \ 10000, \ 16000$ - DNS channel flow (N. Nikitin, private communication).
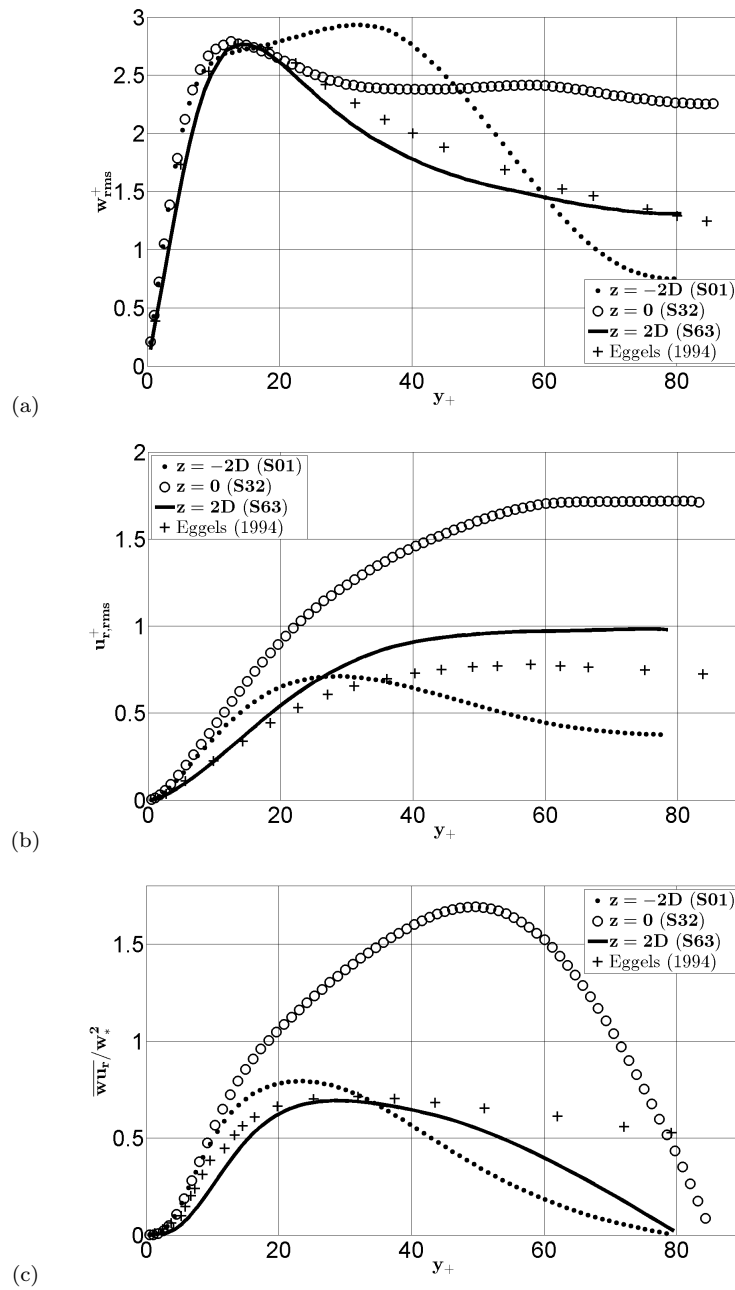
3.3 Turbulence flow intensities

The distribution of the root-mean-square of the fluctuating velocities, normalized by the wall-shear velocity, in wall coordinates are shown in figure 11. For comparison, we present the DNS results of [22] obtained for a fully-developed turbulent flow in a pipe at $Re_m = 5300$ (hereinafter referred to as Eggels94). The root-mean-square (r.m.s) data are averaged over 10000 snapshots and over 78 azimuthal points for each radius (r). For $y_+ < 14$, the streamwise fluctuating velocity intensity w_{rms}^+ practically does not change along the moving window (figure 11a) and reaches the maximum value of 2.8 at $y_+ = 13.8$, which is in remarkable agreement with Eggels94. This is clear evidence that the near-wall streamwise turbulence is formed (locked) at the early stage of transition without being influenced by the energy generation in the core. The streamwise turbulence intensities computed for $y_+ > 20$ considerably differ at different sections. At the moving window trailing edge (figure 11a, S01), w_{rms}^+ has a peak due to high turbulent production in the vicinity of the puff upstream front, as was previously discussed. Further downstream, the streamwise turbulence intensities rapidly redistribute across the pipe, such that they correlate with the Eggels94 results at S63.

Figure 11b shows the r.m.s. of the radial velocity component. The profiles on S32 and S63 are qualitatively similar to those of Eggels94, while $u_{r,rms}^+$ for S63 replicates the Eggels94 results at the near-wall region $0 < y_+ < 18$. Between the moving window trailing edge and middle cross-section, the strong radial motion takes place over the entire cross-section (figure 5c). In addition, as we have seen, u_r and w are also well correlated. This explains the increase of the Reynolds stresses $\overline{wu_r}$ in figure 11c (S32). As a result, in accordance with the energy balance equation (1), the kinetic energy of the streamwise fluctuations $\overline{w^2}$ increases (figure 11a). Further downstream, between the S32 and S63 sections, both, the radial velocity intensity ($u_{r,rms}^+$, figure 11b) and the mean velocity shear (figure 9a) decrease, which, accordingly, leads to a decrease of the Reynolds stress $\overline{wu_r}$ (figure 11c).

3.4 High-order statistics

For each (r, θ) cross-section, we collected 78×78 data points clustered to the wall in the radial direction and equally-spaced in the azimuthal direction for 10000 snapshots, yielding $60,840,000$ sampling points total for statistical analysis. Figures 12 and 13 show the skewness (S) and kurtosis (Ku) factors of the streamwise velocity fluctuations, w, and the normal-to-the-wall velocity component centered around the snapshot-ensemble averaged value, $u_r' = u_r - \overline{u_r}$.

In figure 12, close to the wall, the distributions show positive skewness for u_r', indicating that there are no significant differences for distributions on the S01, S32 and S63 cross-sections. By definition, a positive skewness factor $S(u_r') > 0$ means that the probability distribution function, PDF(u_r'), has a longer tail for $u_r' > 0$ than for $u_r' < 0$. Hence, the events with positive u_r'

(a)

(b)

(c)

Fig. 11 The root-mean-square turbulence intensities (a,b) and Reynolds shear stress (c) normalized by the wall-shear velocity in wall coordinates for different cross-sections along the moving window.

.

are more likely to take place than with negative u'_r. This is what happens due to sweeping a high-speed fluid towards the wall. The same distribution was computed by DNS of a fully-developed turbulent channel flow [24]. DNS results in a pipe (figure 12a, Eggels94) show the opposite, negative $S(u'_r)$ near the wall. Upon publication, this discrepancy has been discussed and can be attributed to the grid spacing near the wall. For example, the first mesh points in Eggels94 and KMM87 were located at $y_+^{(1)} = 1.9$ and $y_+^{(1)} = 0.05$, respectively; in our simulations $y_+^{(1)} \approx 0.5$.

The negative skewness $S(u'_r)$ computed for $y_+ > 30$ at the trailing edge (figure 12a, S01) contradicts the corresponding positive values reported for fully-developed flows in a pipe [22] and in a channel [24]. This is a direct consequence of the difference between the transient and developed turbulence in a pipe. Indeed, $S(u'_r) < 0$ means that events with negative $u'_r < 0$ dominate. In the considered flow, as has been shown, this occurs due to the entrainment of a low-speed fluid lifted-up from the wall by a high-speed flow in the vicinity of the puff upstream edge.

In figure 12b, the distribution of kurtosis $\mathrm{Ku}(u'_r)$ in the near-wall region, $y_+ < 15$, in the sections S01 and S32 coincides with the results of Eggels94. Here, the large kurtosis manifests the extreme sweep/ejection events. Further downstream, the $\mathrm{Ku}(u'_r)$ curve in S32 is consistent with the fully-developed pipe results (Eggels94), while in S01, the curve deviates toward anomalously large values in the pipe core. As with $S(u_r) < 0$ in figure 12a, this is due to the extreme events associated with the penetration of the lifted-up liquid into the center of the pipe. Two diameters downstream (S32 and S63), the distributions of $\mathrm{Ku}(u'_r)$ for $y_+ > 40$ approach the Eggels94 curve following the normal Gaussian.

From figure 13a, near the wall, $y_+ < 10$, $S(w) > 0$ on the S01, S32 and S63 cross-sections. A positive near-wall skewness factor $S(w) > 0$ has been previously computed and experimentally obtained in fully-developed turbulent flows in pipes and channels which confirms the sweeping-like events leading to positive streamwise fluctuations ($w > 0$). This indicates the motion of a high-speed fluid towards the wall. On the trailing edge (S01), we indicate one crossover, $S(w)=0$ at $y_+ = 10$, followed by a considerable departure of $S(w)$ for $y_+ > 30$ towards a large negative value of -3.8 at the pipe center. Hence, the events with large negative $w < 0$, are more likely to take place there. The events with $S(w) < 0$ and $S(u'_r) < 0$ happen due to the lift-up of a low-speed fluid from the wall to the center.

The processes dominated by intermittent extreme events has high kurtosis. The flow at the puff upstream edge (S01) is highly intermittent due to its laminar-turbulent nature, which is manifested in figure 13b by an abnormally high kurtosis factor $\mathrm{Ku}(w)$ at $y_+ > 40$. It is very remarkable that four diameters downstream (S63) the kurtosis curve approaches the normal Gaussian distribution value of Ku=3 for most of the cross-section (figure 13b), which is in full agreement with the results obtained for fully-developed turbulent pipe flow [22].

(a)

(b)
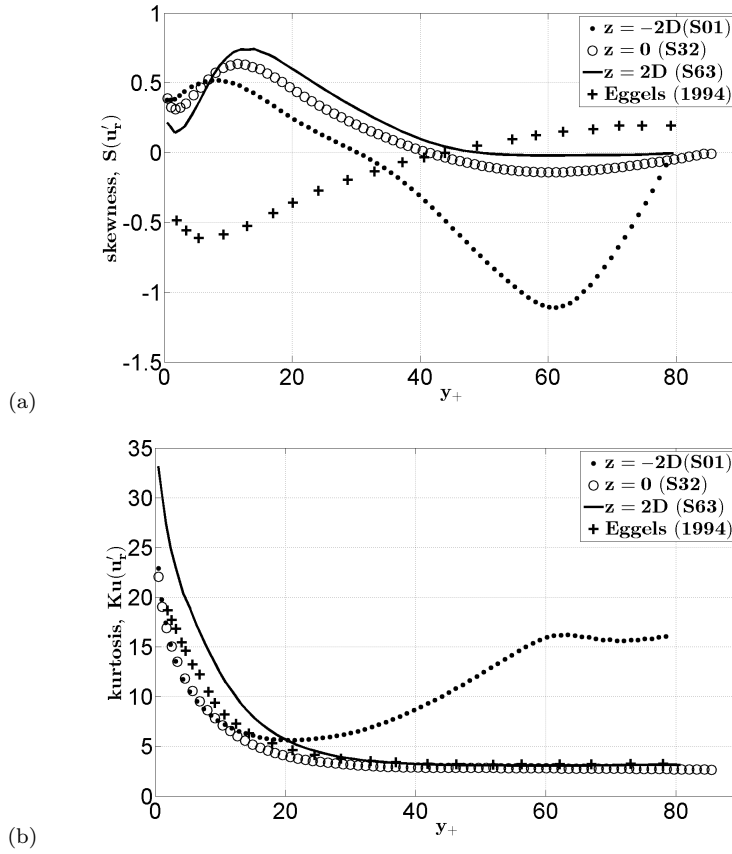
Fig. 12 Skewness (S) and kurtosis (Ku) factors of the normal-to-the-wall velocity fluctuations in wall coordinates; $u'_r = u_r - \overline{u_r}$.
.

4 Discussion and summary

The purpose of this study is to analyze turbulence in a localized puff for a threshold Reynolds number before it expands in the streamwise direction into a slug. In [14], based on extensive studies, this Reynolds number was established as $Re_m = 2250$. In our study, the data was accumulated over the time interval of $T = 2000D/U_m$ and no puff splitting or length change occurred, indicating that it remained localized. As was shown in [9], at Re=2250, puffs will almost certainly never decay and will split after an average of about 5500 time units (albeit with a rather large range of uncertainty). For L=90D, a puff is surrounded by a fully laminar flow, that is, the only mechanism for sustaining the turbulence inside a puff is that a high-speed laminar fluid passes through it [8]. For a shorter pipe, figure 3 indicates a 10% deficit in streamwise velocity, indicating that the flow behind the puff is not completely relaminarized. The

(a)

(b)
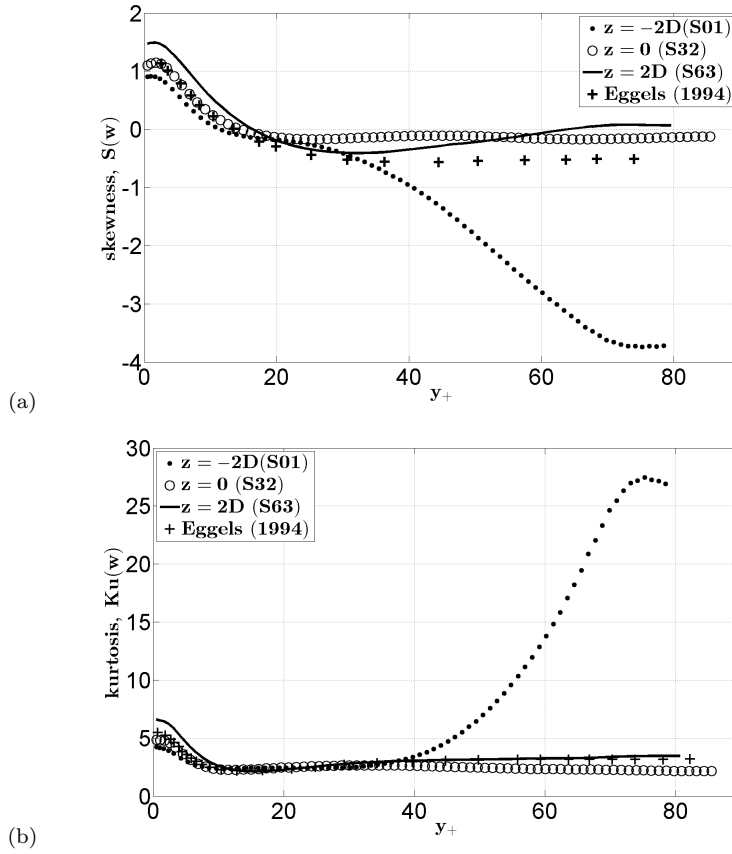
Fig. 13 Skewness (S) and kurtosis (Ku) factors of the streamwise velocity fluctuations in wall coordinates.
.

time trace in figure 3 replicates those obtained in [8] for Re=2350 and L=90D after several puff splits, indicating that the flow dynamics is not fully isolated, but rather corresponds to a chain of weakly interacting puffs. Evidently, this is how we should consider the results of our study; namely, as the characteristics of a single, but not a completely isolated puff. The case with a longer domain (L=70÷90D, Re=2250) still remains to be investigated in order to understand whether it does affect the near-wall distributions of the turbulence intensities and high-order statistics (skewness and flatness factors) inside a puff.

In figure 14a, there are two counter-rotating streamwise vortices, viz., one clockwise rotating (3), the other counter-clockwise rotating (1). Both correspond to lifting up the low-speed fluid in those locations shown in figure 14c. Analyzing the ω_z and u_θ patterns supports the development of the radial motion which yielded to the wavy w-pattern in figure 4b. Some comments on the symmetrical footprints (1 and 3) in figure 14c are called for. We focused

on the velocity inside the moving window. The development of axial vorticity near the wall is confirmed by our results (figure 14a). As for clear confirmation whether this is the beginning of the development of "hairpin-like" vortices, this cannot be asserted in the chosen moving window. On the other hand, we see vestiges of the axial vortical motion in the form of the elongated "finger-like" structures that appeared after long-time averaging (figure 2).

Figure 14b reveals quite intensive counter-directional azimuthal motion near the wall. Moreover, the u_θ-pattern replicates the ω_z pattern. Note a quite long $\omega_z = 0$ interface line which is the signature of the inflexion point in the velocity profile.

The computational domain steamwise period, $L = 25D$, has been claimed to be a minimal admissible pipe length [11]. In support of this, our description of the development of flow structures inside a puff is in full agreement with [6]. Thus, we do not recognize the influence of the computational domain length used in this study on the laminar-turbulent transition scenario thoroughly described in previous computational and numerical studies. A possible influence of the periodicity length on turbulent characteristics obtained inside a puff deserves comment. The laminar (Poiseuille) centerline velocity normalized by U_m is 2. From figure 3, the flow behind a puff is not completely relaminarized. Figure 15a shows the distribution of the Reynolds stress $\overline{wu_r}$ computed 14 diameters downstream ($z = 12D$) and 4 diameters upstream ($z = -6D$) of the moving window trailing edge ($z = -2D$, $S01$). Indeed, upstream of S01, the centerline velocity shows a 10% deficit (figure 15b), while the level of the near-wall Reynolds stress is practically insignificant (figure 15a). It is noteworthy that at S01, the mean velocity profile shows the trace of the inflexion point at $r \simeq 0.3$ (figure 15b), marking the beginning of the laminar-turbulent transition.

For DNS of fully-developed turbulent pipe flows, periodic boundary conditions are imposed in the axial direction while the length (L) of the computational domain (period) is made by examining the experimental data, in particular, by two-point correlation measurements. This means that the results must be uncorrelated at a distance of the periodicity length. In [22] and [24], $L = 5D$ and $L = 2\pi H$ (H is the channel width), respectively. Figure 16 shows contours of a two-point correlation coefficient between the in-plane velocity components, R_{u_r,u_r} and R_{u_θ,u_θ}, at the moving window trailing edge ($z = -2D$) and 14 diameters downstream. The results show the level of correlation is quite low.

The snapshot-ensemble averaging over all 10000 snapshots revealed 5 azimuthally placed structures as marked in figure 6a. At S01, the pipe radius measured in wall units is about $Re_\tau \approx 80$. Thus, five structures in figure 6a separate the near-wall streaks with streak spacing of $\Delta l_+ \approx 100$ in wall units.

Figures 17a-c depict contours of the instantaneous radial velocity for three time instances from the interval $1200D/U_m \leq T \leq 1300D/U_m$. Figure 17d shows the contours of radial velocity averaged over this interval, $\Delta T = 100D/U_m$. Here, the marks 1÷5 correspond to those in figure 6a. The same pattern, as that in figure 6a obtained by averaging over the entire interval of $\Delta T =$
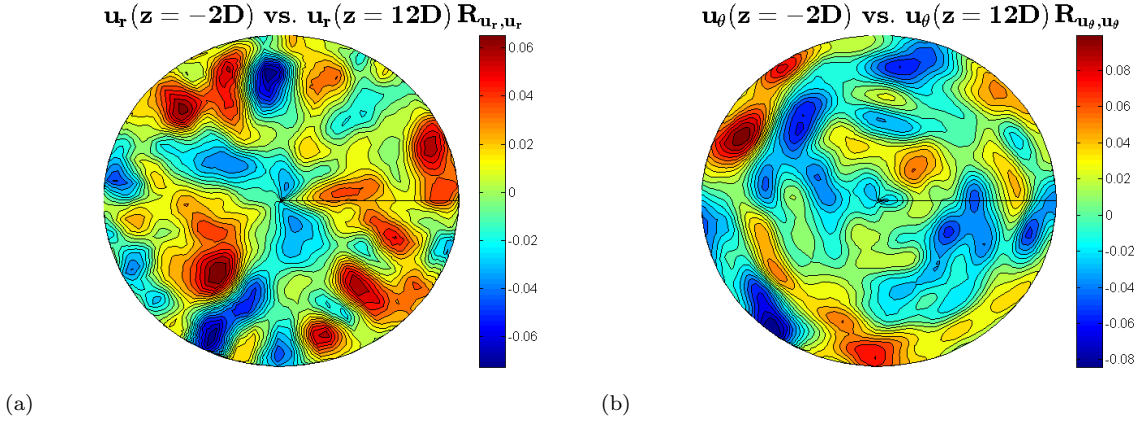
(a)

(b)

(c)
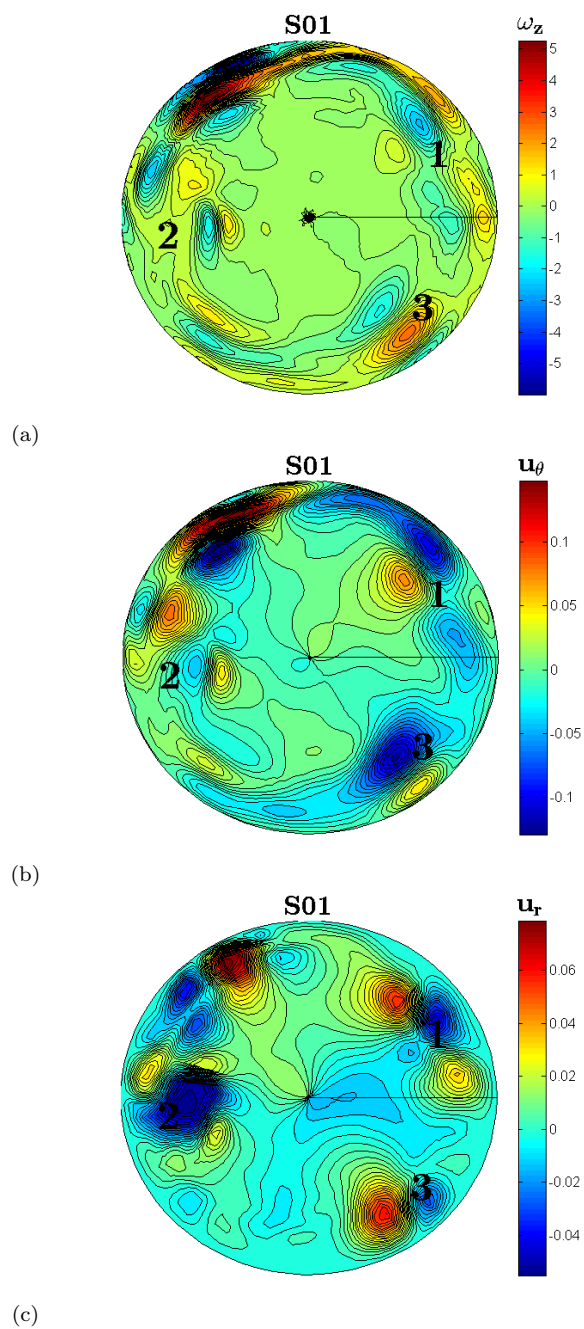
Fig. 14 Contours of the instantaneous axial vorticity ω_z (a), azimuthal velocity u_θ (b), and radial velocity u_r (c) at the moving window trailing edge S01, the marks correspond to the same locations; the corresponding u_z- and $w-$components are shown in figure 4.
.

(a)

(b)
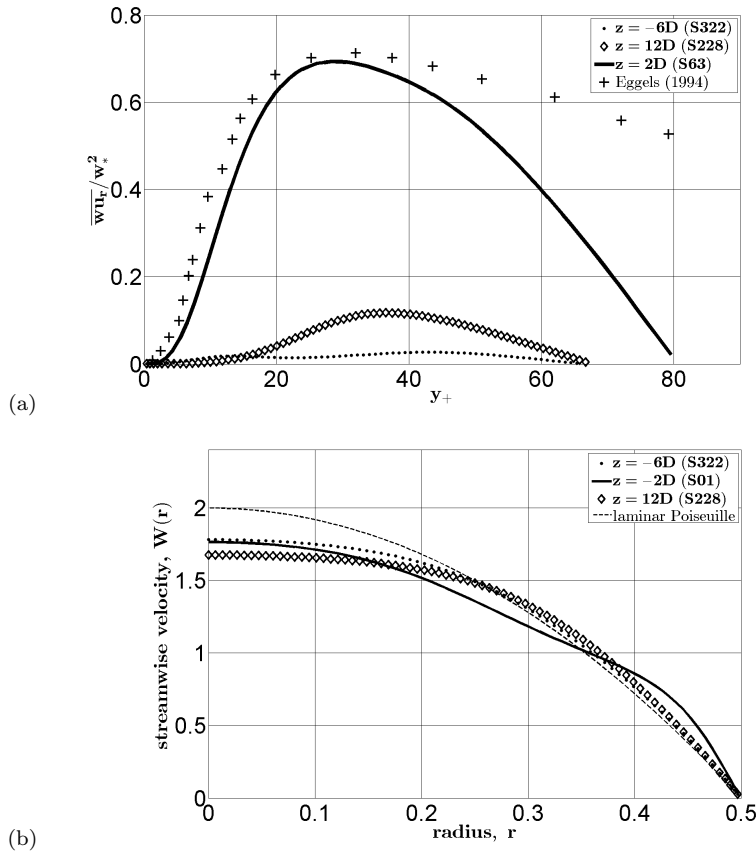
Fig. 15 The Reynolds shear stress (a) normalized by the wall-shear velocity in wall co-ordinates and the streamwise velocity profile normalized by the mean velocity (b) for different pipe cross-sections downstream and upstream of the moving window trailing edge ($z = -2D$).
.

$2000D/U_m$, can be observed in figure 17d obtained for $\Delta T = 100D/U_m$. Some footprints (1 and 2) are very well pronounced, some less (3, 4 and 5), but all five appear after long-time averaging as shown in figure 6a. From comparison of figures 6a and 17d, it follows that after averaging over the intervals of $\Delta T = 100D/U_m$ and $\Delta T = 2000D/U_m$ an azimuthally asymmetrical radial motion persists on these time scales. Consequently, the same regarding the streamwise vortices, since their existence is connected with the radial velocity $\theta-$dependency. As we noted, it is plausible that the extremely long-time averaging should produce azimuthally symmetric properties. The question what should be the averaging interval to give azimuthally symmetric distributions, and whether it exists at all within the framework of our computational setup, is beyond the scope of this study.

$\mathbf{u_r(z = -2D)}$ vs. $\mathbf{u_r(z = 12D)}$ $\mathbf{R_{u_r,u_r}}$ **$\mathbf{u_\theta(z = -2D)}$ vs. $\mathbf{u_\theta(z = 12D)}$ $\mathbf{R_{u_\theta,u_\theta}}$**

(a)   (b)

Fig. 16 Contours of a two-point correlation coefficient between the cross-plane velocity components at the moving window trailing edge ($z = -2D$) and 14 diameters downstream.
.

Figure 18a shows the instantaneous streamwise velocity u_z at the moving window trailing edge. Here, 5 near-wall streaks can be recognized. The two-point azimuthal correlation coefficient of the streamwise velocity, $R_{u_z,u_z}(\theta, \theta_0)$ is shown in 18b. For $\theta_0 = 350°$, the radius $r = 0.25$ yields a maximum azimuthal correlation, that is, $R_{u_z,u_z}(206°, 350°) = -0.22$. From figure 18a, these two locations correspond to the high-speed fluid sweeping towards the the wall ($r = 0.25, \theta_0 = 350°$) and the low-speed fluid ejection from the wall ($r = 0.25, \theta_0 = 206°$) indicating that these two events are correlated. A similar correlation has been experimentally obtained in [20], which supports the existence of travelling waves in pipe flow.

In this paper we have studied the flow structure in a localized puff using a moving window (co-moving frame of reference) approach, focusing on the analysis of the flow field data inside a 4D-length window centered at the location of the maximum cross-plane kinetic energy. The trailing edge of the moving window is 2D upstream; the upstream edge of the puff is about 3D upstream (figure 3). At this location, the streamwise mean velocity profile showed an inflexion point which appeared as a result of an ejection of low-speed fluid from the wall into the pipe center. It is noteworthy that the location of the inflexion point of $r \approx 0.3$ or $y_+ \approx 33$ in wall units (S01 profile in figure 15b), coincides with the location of the energy peak of streamwise fluctuations (S01 profile in figure 11a), which agrees with the observation of [7]. In the puff core, the velocity profile becomes flat and logarithmic. The results indicated that this "fully-developed turbulent flash" is very narrow, being about two pipe diameters long.

We computed long-time statistical and averaged properties. In the near-wall region, despite a low Reynolds number, the turbulence statistics, in particular, the distribution of turbulence intensities and Reynolds shear stress turns out to be similar to a fully-developed turbulent pipe flow just in the vicinity of

(a)

(b)

(c)

(d)
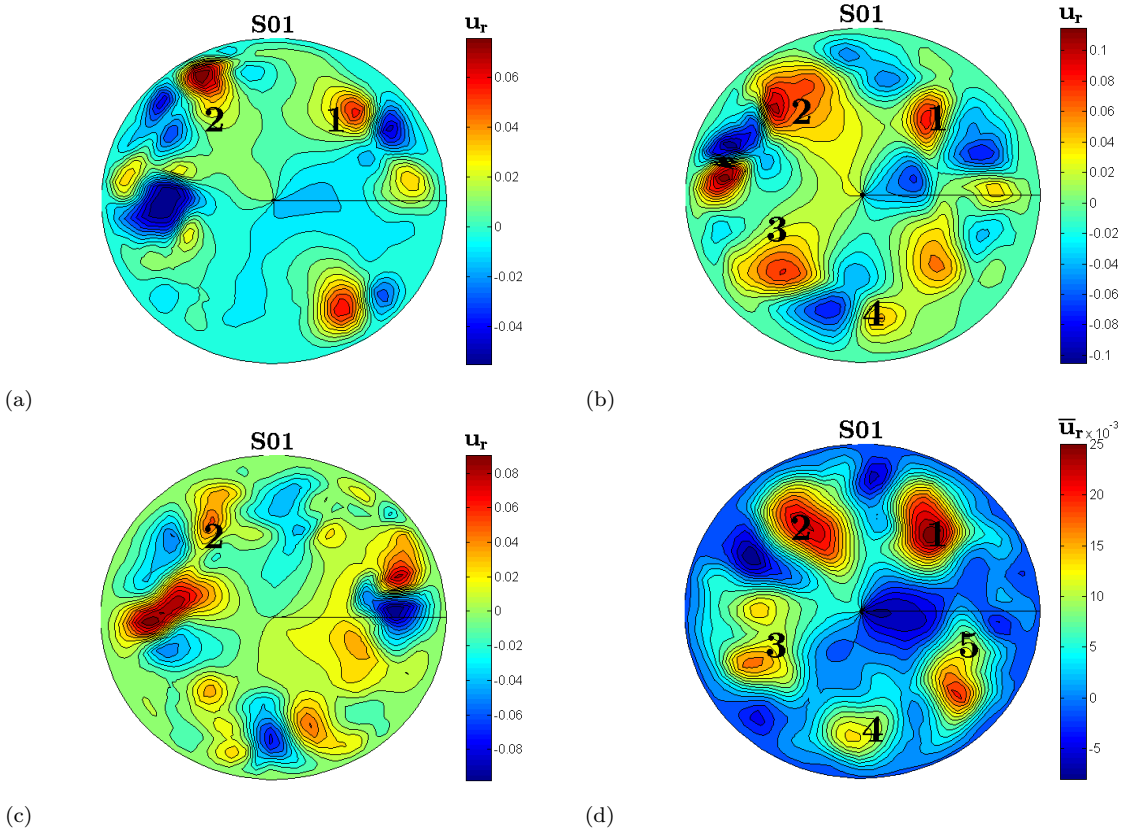
Fig. 17 Contours of the instantaneous radial velocity (u_r) at different time instances: $T = 1200$ (a), $T = 1250$ (b), $T = 1300$ (c), and (d) averaged over consequent 500 snapshots corresponding to the $\Delta T = 100$ time interval $1200 \leq T \leq 1300$.
.

the puff upstream edge. For shear flows, in particular, in a pipe, the turbulent intensity level of the streamwise component is the highest, while the cross-plane energy is generated by the pressure-strain interaction. Our results show that the near-wall distribution of the turbulence streamwise intensity r.m.s. practically does not change along a $4D$-width moving window. Moreover, for $0 < y_+ < 15$, this distribution is similar to a fully-developed turbulent pipe flow.

The near-wall distributions of the skewness (S) and kurtosis (Ku) factors obtained along the moving window agree with those obtained for fully-developed pipe flows. The anomalous distributions of S and Ku in the pipe core in the vicinity of the puff upstream edge represent the quantification of the intermittent flow regime there.
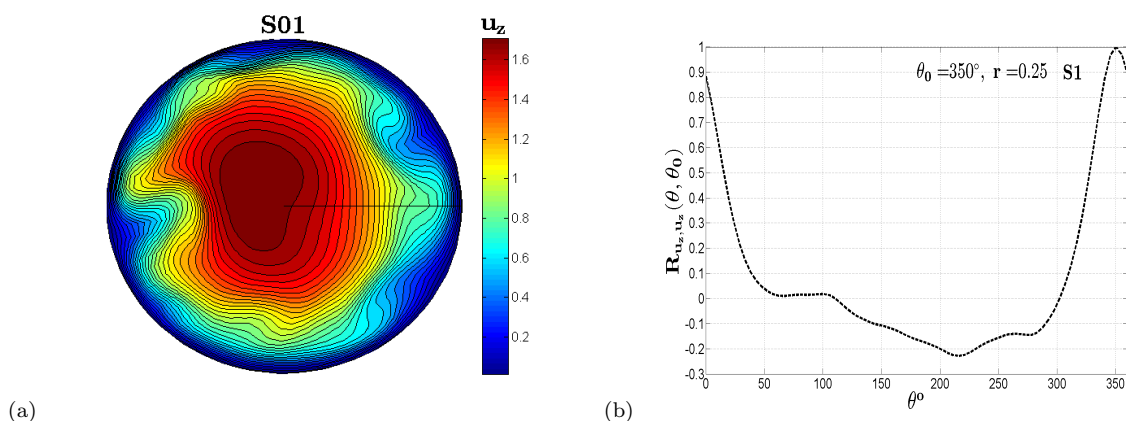
Fig. 18 (a) Typical contours of the instantaneous streamwise velocity (u_z) at the moving window trailing edge S01 and (b) the two-point correlation coefficient R_{u_z,u_z} calculated in the azimuthal direction for a specified radius r.
.

Acknowledgements

Conflict of interests

The authors declare that they have no conflict of interest.

References

1. Barkley, D., Song, B., Mukund, V., Lemoult, G., Avila, M. & Hof, B. 2015 The rise of fully turbulent flow. *Nature* **526**, 550–553.
2. Barkley, D., Song, B., Mukund, V., Lemoult, G., Avila, M. & Hof, B. 2015 The rise of fully turbulent flow. Available from: https://arxiv.org/pdf/1510.09143.pdf.
3. Wygnanski, I. J. & Champagne, F. H. 1973 On transition in a pipe. Part 1.The origin of puffs and slugs and the flow in a turbulent slug. *J. Fluid Mech.* **59**, 281–335.
4. Wygnanski, I. J., Sokolov, M. & Friedman, D. 1975 On transition in a pipe. Part 2. The equilibrium puff. *J. Fluid Mech.* **69**, 283–304.
5. Barkley, D. 2016 Theoretical perspective on the route to turbulence in a pipe. *J. Fluid Mech.* **803**, P1–80.
6. van Doorne, C. W. H. & Westerweel, J. 2009 The flow structure of a puff. *Phil. Trans. R. Soc. Lond. A* **367**, 1045–1059.
7. Hof, B., de Lozar, A., Avila, M., Tu, X. & Schneider, T. 2010 Eliminating turbulence in spatially intermittent flows. *Science* **327**, 1491–1494.
8. Moxey, D. & Barkley, D. 2010 Distinct large-scale turbulent-laminar states in transitional pipe flow. *PNAS* **107**, 8091–8096.
9. Avila, K., Moxey, D., de Lozar, A., Avila, M., Barkley, D. & Hof, B. 2011 The onset of turbulence in pipe flow. *Science* **333**, 192–196.
10. Shan, H., Ma, B., Zhang, Z. & Nieuwstadt, F. T. M. 1999 On transition in a pipe. Part 2.Direct numerical simulation of a puff and a slug in transitional cylindrical pipe flow . *J. Fluid Mech.* **387**, 39–60.
11. Priymak, V. & Miyazaki, T. 2004 Direct numerical simulation of equilibrium spatially localized structures in pipe flow. *Phys. Fluids* **16**, 4221—4234.

12. Priymak, V. & Miyazaki, T. 1994 Long-wave motions in turbulent shear flows. *Phys. Fluids* **6**, 3454–3464.
13. Shimizu, M. & Kida, S. 2009 A driving mechanism of a turbulent puff in pipe flow. *Fluid Dyn. Res.* **41** (4), 045501.
14. Song, B., Barkley, D., Avila, M. & Hof, B. 2017 Speed and structure of turbulent fronts in pipe flow. *J. Fluid Mech.* **813**, 283–304.
15. Blackburn, H. M. & Sherwin, S. J. 2004 Formulation of a Galerkin spectral element-Fourier method for three-dimensional incompressible flows in cylindrical geometries. *J. Comp. Phys.* **197**, 759–778.
16. Karniadakis, G. E., Israeli, M. & Orszag, S. A. 1991 High-order splitting methods for the incompressible Navier-Stokes equations. *J. Comp. Phys.* **97**, 414–443.
17. Chu, D., Henderson, R. & Karniadakis, G. E.. 1992 Parallel spectral-element-Fourier simulation of turbulent flow over riblet-mounted surfaces. *Theo. Comp. Fluid Dyn.* **3**, 219–229.
18. Moxey, D. 2011 Spatio-temporal dynamics in pipe flow. *PhD thesis, University of Warwick.*
19. Moser, R. D. & Moin, P. 1984 Direct numerical simulation of curved turbulent channel flow. *NASA Technical Memorandum* 85974, 84–87.
20. Hof, B., van Doorne, C. W. H., Westerweel, J., Nieuwstadt, F. T. M., Faisst, H., Eckhardt, B, Wedin, H., Kerswell, R. R. & Waleffe, F. 2004 Experimental observation of nonlinear traveling waves in turbulent pipe flow. *Science* **305**, 1594–1598.
21. Willis, A. R. & Kerswell, R. R. 2008 Coherent structures in localized and global pipe turbulence. *Phys. Rev. Lett.* **100**, 124501.
22. Eggels, J. G. M., Unger, F., Weiss, M. H., Westerweel, J., Adrian, R. J., Friedrich, R. & Nieuwstadt, F. T. M. 1994 Fully developed turbulent pipe flow: a comparison between direct numerical simulation and experiment. *J. Fluid Mech.* **268**, 175–209.
23. Moser, R. D., Kim, J. & Mansour, N. N. 1999 Direct numerical simulation of turbulent channel flow up to $Re_\tau = 590$. *Phys. Fluids* **11** (4), 943–945.
24. Kim, J., Moin, P. & Moser, R. D. 1987 Turbulence statistics in fully developed channel flow at low Reynolds number. *J. Fluid Mech.* **177**, 133–166.